Proceedings of the 56th Israel Annual Conference on
Aerospace Sciences, Tel-Aviv & Haifa, Israel
March 9-10, 2016

Stability of streaks in shear flows

M. Karp[1]*, J. Philip[2]† and J. Cohen[1]‡

[1] *Faculty of Aerospace engineering, Technion - Israel Institute of Technology, Haifa 32000, Israel*

[2] *Department of Mechanical Engineering, University of Melbourne, VIC 3010, Australia*

The stability of streaks, generated by vortices in wall-bounded shear flows, is studied analytically, numerically and experimentally. A novel analytical approximation of the linear transient growth in Couette flow allows investigating the secondary stability of spanwise periodic streaks using Floquet theory. The optimal parameters for instability correspond to the strongest inflection points, those having maximal shear, rather than initial conditions maximizing the energy growth. For the symmetric transient growth the most dangerous secondary disturbances are sinuous, associated with spanwise inflection points having a spanwise wavenumber of $\beta = 3.6$ (as opposed to $\beta = 1.67$ which maximizes energy growth) and the varicose instabilities are associated with spanwise inflection points as well. For the antisymmetric transient growth both sinuous and varicose instabilities are observed, associated with spanwise and wall-normal inflection points, respectively. The theoretical results are verified by obtaining transition in a direct numerical simulation (DNS) initiated by the corresponding analytical expressions. The rapid evolution of the secondary disturbance on top of the slowly evolving transient growth enables us to use the multiple time scales method to follow the evolution of the secondary disturbance. The very good agreement between the DNS and analytical expressions verifies the theoretical predictions. Finally, the above results are discussed with respect to previous transitional pipe and Poiseuille flow experiments.

I. Introduction

Streaks of high and low velocity appear in various flow states, both in laminar flow, where they may be created by wall blowing, suction or by the presence of a bump, as well as in transitional and turbulent flows (e.g. [1,2]). In particular, streamwise independent streaks have been identified as the ones responsible for maximal transient growth (TG), which has been proposed as a route to turbulence in wall-bounded shear flows. A significant TG of several orders of magnitude can occur for linearly stable flows [3]. Consequently, the stable flow is modified and may become linearly unstable to secondary instabilities. The optimal linear TG corresponds to a symmetric pair of nearly streamwise independent counter rotating vortices (CVP), having a spanwise wavenumber of $\beta = 1.67$ for Couette flow [3]. Additionally, there exists also an antisymmetric optimum consisting of two pairs of CVPs (four vortices); however the latter grows much less than the symmetric optimum. The vortices create streaks which may introduce instability to

*PhD. Student, mkarp@technion.ac.il
†Lecturer, jimmyp@unimelb.edu.au
‡Professor, aerycyc@gmail.com

the flow. The secondary instability of streaks in channel flows has been investigated by Reddy *et al.* [4] for the symmetric optimum and a single wavenumber of $\beta = 2$ (this value yields maximal energy gain for Poiseuille and almost maximal energy gain for Couette flow). Recently, Karp and Cohen [5] have demonstrated that maximal energy growth is not essential for obtaining transition. Rather, it is the ability of the modified base-flow to create strong enough inflection points in the velocity profile. This has been demonstrated by simulating the transition process in Couette flow undergoing antisymmetric TG where the maximal energy gain has been an order of magnitude smaller than that associated with the symmetric optimal for the same flow parameters.

In this work, the model of Karp and Cohen [5] is utilized to find the optimal wavenumbers (β) which maximize the shear at the inflection points. At the next step, the most dangerous secondary disturbances, having the highest growth rate, for symmetric and antisymmetric TG are identified. The route to turbulence of each of the disturbances is then explored via DNS and compared an analytical approximation based on the multiple time scales method. Finally, the scope is broadened and the results are compared to previous transitional pipe and Poiseuille flow experiments.

II. Mathematical Model and DNS

The TG in Couette flow is approximated analytically by a combination of four stable modes. The model is summarized below, while further details can be found in [5]. TG is usually characterized by the gain of the kinetic energy:

$$E(t) = \frac{1}{4L_xL_z}\int_0^{L_z}\int_{-1}^{1}\int_0^{L_x}(u^2+v^2+w^2)dxdydz; \qquad G(t) = \frac{E(t)}{E_0}, \tag{1}$$

where $E(t)$ is the kinetic energy, given by a volumetric integral over the whole domain and $G(t)$ is the energy gain, which is the energy normalized by its initial value $E_0 = E(t=0)$. The velocity field is $\boldsymbol{u}(t,x,y,z) = (u,v,w)^T$, where t is the time and u, v, w are the velocity components in the streamwise, wall-normal and spanwise coordinates (x,y,z), respectively. All length scales are normalized by the channel half height, h. The velocity is normalized by the velocity of the wall, U_w and time by h/U_w. The velocity field is described by

$$\boldsymbol{u} = \boldsymbol{U}_0(y) + \varepsilon\boldsymbol{u}_1(t,y,z) + \varepsilon^2\boldsymbol{u}_2(t,y,z) + \delta\boldsymbol{u}_d(t,x,y,z) + \cdots, \tag{2}$$

where $\boldsymbol{U}_0(y) = (y,0,0)^T$ is the Couette base-flow. The term $\varepsilon\boldsymbol{u}_1(t,y,z)$ represents the linear TG disturbance which is a combination of four modes, $\varepsilon^2\boldsymbol{u}_2(t,y,z)$ represents the nonlinear TG modification consisting of the interactions between the four modes and $\delta\boldsymbol{u}_d(t,x,y,z)$ represents the secondary $3d$ disturbance. The need to calculate the nonlinear modification of the TG ($\boldsymbol{u}_2$) arose in our previous work [5], where its inclusion was essential for obtaining instability in the case of antisymmetric TG. The $O(\varepsilon^2)$ equations are solved analytically using Duhamel's principle. It is convenient to designate the Couette flow undergoing TG, i.e. the modified base-flow, as:

$$\boldsymbol{U}(t,y,z) = \boldsymbol{U}_0(y) + \varepsilon\boldsymbol{u}_1(t,y,z) + \varepsilon^2\boldsymbol{u}_2(t,y,z). \tag{3}$$

A. Multiple time scales

The TG is initially algebraic, followed by slow viscous decay over a long time scale of $O(Re)$. Except the initial stage, a separation of time scales between the slowly varying TG

and a rapidly evolving secondary disturbance can be assumed. In our previous work [5], it has been assumed that the secondary disturbance evolves with a constant eigenvalue and eigenfunction. In the current study the model is improved with the aid of the multiple time scales method. Accordingly, the velocity field is written as

$$\boldsymbol{u} = \boldsymbol{U}(\tau, y, z) + \delta \boldsymbol{u}_d(t, \tau, x, y, z) + \mu\delta \boldsymbol{u}_{dd}(t, \tau, x, y, z) + \cdots , \tag{4}$$

where $\tau = \mu t$ is the slow time scale ($\mu = O(Re^{-1}) \ll 1$), $\boldsymbol{U}(\tau, y, z)$ is the modified base-flow which depends only on the slow time scale, $\delta \boldsymbol{u}_d(t, \tau, x, y, z)$ is the secondary disturbance which depends on both time scales and $\mu\delta \boldsymbol{u}_{dd}(t, \tau, x, y, z)$ is used to correct the long time evolution of the secondary disturbance. Following the multiple time scales method, we assume

$$\boldsymbol{u}_d = \Re\left\{ A(\tau) \exp\left\{ i\left(\alpha x - \frac{1}{\mu}\int_{\mu t_0}^{\mu t} \omega(\tau) d\tau \right) \right\} \sum_{k=-M_z}^{M_z} \hat{\boldsymbol{u}}_{d_k}(\tau, y) e^{i\beta k z} \right\}, \tag{5}$$

where α is the streamwise wavenumber, $\omega(\tau)$ the slowly varying eigenvalue, $\hat{\boldsymbol{u}}_{d_k}(\tau, y)$ the slowly varying eigenfunction and $A(\tau)$ the slowly varying amplitude.

Substituting expression (4) into the Navier Stokes equations we obtain:
(a) the $O(\mu, \mu^2)$ equations governing the evolution of the modified base-flow $\boldsymbol{U}(\tau, y, z)$;
(b) the $O(\delta)$ equations for the secondary disturbance $\boldsymbol{u}_d(t, \tau, x, y, z)$ which have already been solved using Floquet theory in our previous work [5], where the modified base-flow has been assumed to be parallel and frozen in time (see eq. (2.6) and appendix C therein);
(c) the $O(\mu\delta)$ equations for the slow time correction of the secondary disturbance. These equations for $\boldsymbol{u}_{dd}$ are used to obtain the correction of the amplitude $A(\tau)$ for long times and are detailed in appendix A. This procedure involves the calculation of the adjoint eigenfunctions which is detailed in appendix B. The amplitude correction is given by

$$A(\tau) = A_0 \exp\left(-\int_{\tau_0}^{\tau} \frac{N(t')}{M(t')} dt' \right), \tag{6}$$

where A_0 is the initial amplitude at time τ_0. Substituting eq. (6) back into the expression for the secondary disturbance (eq. (5)) we obtain:

$$\boldsymbol{u}_d(t, x, y, z) = \Re\left\{ A_0 \exp\left(i\left(\alpha x - \Theta(t) \right) \right) \sum_{k=-M_z}^{M_z} \hat{\boldsymbol{u}}_{d_k}(t, y) e^{i\beta k z} \right\}, \tag{7a}$$

$$\Theta(t) = \int_{t_0}^{t} \left(\omega(t') - \frac{i}{Re} \frac{N(t')}{M(t')} \right) dt', \tag{7b}$$

where $\Theta(t)$ is the secondary disturbance phase, corrected for long times. When calculating the evolution of the secondary disturbance, first the eigenvalues $\omega(t)$ and eigenfunctions $\hat{\boldsymbol{u}}_{d_k}(t, y)$ are obtained using the secondary stability analysis. The eigenfunctions are normalized by the value of the streamwise eigenfunction at a certain location (y_0, z_0) to ensure that they change smoothly with time. It should be noted that as the multiple scales analysis is linear, the results are independent of the location of the normalization (y_0, z_0).

The next stage is the calculation and normalization of the adjoint eigenfunctions, in a manner similar to the regular eigenfunctions. It should be noted that the adjoint eigenfunctions can be normalized at a location different from the one corresponding to

the regular eigenfunctions. The adjoint eigenfunctions are used to calculate the phase correction term $N(t)/M(t)$, providing the full solution of the secondary disturbance from eq. (7a).

B. Direct Numerical Simulation

The theoretical predictions are compared with results obtained by the 'Channelflow' DNS code [6] initiated by the analytical expressions. The simulation is pseudospectral, utilizing Fourier modes in the x and z directions and Chebyshev modes in y. The results are obtained using $N_x = 64$, $N_y = 65$ and $N_z = 64$. The effect of increasing the resolution is found to be negligible. The domain contains two walls at $y = \pm 1$, a single wavelength in the streamwise direction, $L_x = 2\pi/\alpha$, and a single wavelength in the spanwise direction, $L_z = 2\pi/\beta$. Since the 3/2 rule is applied to remove aliasing, the number of corresponding Fourier modes is $N'_{x,z} = 2/3N_{x,z}$. The time step is chosen to obtain an initial CFL number of ~ 0.1.

III. Results

Using our model we obtain an analytical approximation of the modified base-flow for the symmetric (even) and antisymmetric (odd) TG. The streamwise component of the modified base-flow for the arbitrary chosen values $Re = 1000$, $E_0 = 10^{-4}$, $\beta = 1$ and $t = 30$ is presented in figure 1 for the even (1a) and odd (1b) TG. The color indicates the magnitude of velocity. The strongest wall-normal inflection points, having the maximum wall-normal shear, are indicated by the black circles and the strongest spanwise inflection points, having the maximum spanwise shear, by the magenta circles. The one-dimensional ($1d$) velocity profiles containing the strongest inflections are indicated on the figure.

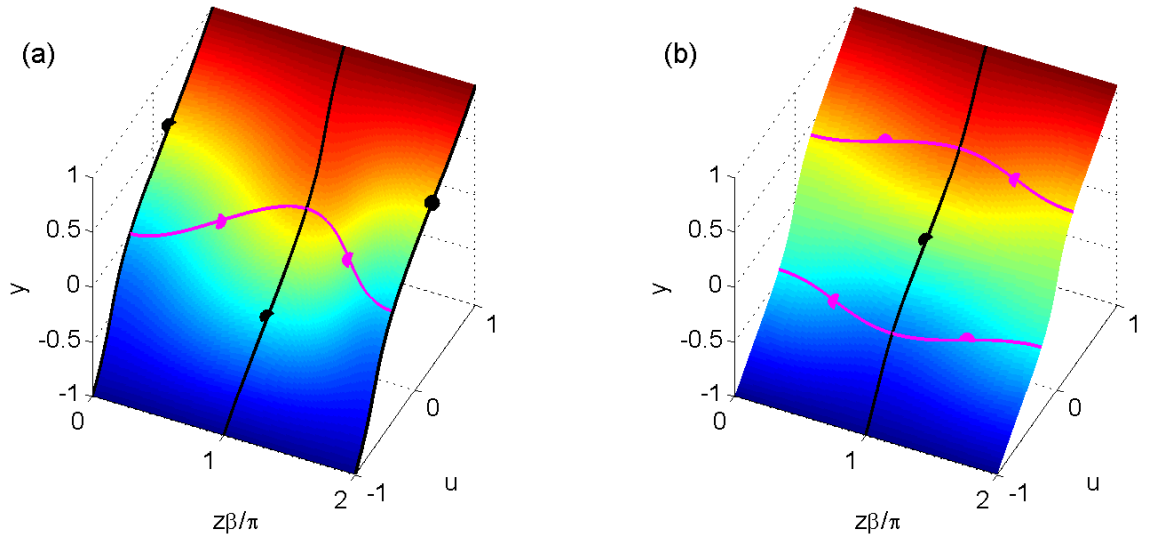

Figure 1. Streamwise modified base-flow for $Re = 1000$, $E_0 = 10^{-4}$, $\beta = 1$ and $t = 30$. The 'strongest inflection' $1d$ velocity distributions in the wall-normal (black) and spanwise (magenta) directions are indicated on the modified base-flow with the strongest inflections encircled. The color indicates the magnitude of velocity. (a) even TG (b) odd TG.

Our purpose is to find the optimal spanwise wavenumbers which maximize the strength of the inflection points (i.e. their shear) over all times. This is achieved by calculating the strongest inflection points for different times and wavenumbers (β, t) and looking for the ones having maximal shear. The resulting strongest inflection points for the even and odd TG, $Re = 1000$ and $E_0 = 10^{-4}$ are presented in table 1. It can be seen that the strongest inflection points, i.e. the ones having maximum shear, are in the wall-normal direction and that the even TG generates stronger inflection points compared to the odd TG. The strongest inflection point are attained for spanwise wavenumbers which do not maximize the energy gain (which is maximized at $\beta = 1.67$ for the even TG and $\beta = 2.8$ for the odd TG).

TG	$\max \frac{\partial U}{\partial y}$	$\beta_{\max \frac{\partial U}{\partial y}}$	$t_{\max \frac{\partial U}{\partial y}}$	$\max \frac{\partial U}{\partial z}$	$\beta_{\max \frac{\partial U}{\partial z}}$	$t_{\max \frac{\partial U}{\partial z}}$
even	3.470	1.8	148	2.247	3	75
odd	2.688	3.3	36	1.176	5.2	25

Table 1. The shear at the strongest wall-normal and spanwise inflection points and the optimal wavenumbers β and times t when it is attained for even and odd TG, $Re = 1000$ and $E_0 = 10^{-4}$.

Type	TG	β	α	t	$\lvert\omega_r/\alpha\rvert$	ω_i
sin.	even	3.6	1.8	61	0	0.311
var.	even	2.1	2.5	81	0.088	0.173
sin.	odd	3.5	1.5	36	0.413	0.092
var.	odd	1.6	1.2	43	0	0.063

Table 2. The optimal parameters yielding the maximal growth rate of the secondary disturbance for $Re = 1000$ and $E_0 = 10^{-4}$ for even and odd TG.

To check whether the strongest inflection points introduce instability to the flow we perform a thorough secondary stability investigation to find the secondary disturbances having the highest growth rate. The parameter space (α, β, t) is explored to find the optimal secondary disturbances for $Re = 1000$ and $E_0 = 10^{-4}$. There are two types of secondary disturbances: varicose and sinuous modes, corresponding to their spanwise distribution: symmetric and antisymmetric, respectively. The parameters maximizing the growth rate of the varicose and sinuous secondary disturbances for the even and odd TG are listed in table 2. It can be seen that the most dangerous secondary disturbance is sinuous and that the even TG has stronger instabilities. For both sinuous disturbances the spanwise wavenumbers are very similar and $\alpha/\beta \sim 2$, while for the varicose disturbances $\alpha \sim \beta$. The optimal spanwise wavenumbers which maximize the secondary instability are different from the ones maximizing the inflection points due to $2d$ effects of the base-flow. Nevertheless, examination of the eigenfunctions of the most dangerous disturbances reveals their connections to inflection points. The streamwise magnitude of the above four secondary disturbances is presented in figure 2. The varicose disturbance (figure 2a, even TG) is associated with spanwise inflections. The combination of a varicose mode and spanwise inflection is somewhat surprising. Therefore this disturbance is compared with a sinuous disturbance calculated for the same parameters ($\alpha = 2.5, \beta = 2.1$ and

$t = 81$). It is found that for these parameters, which maximize the varicose instability, the sinuous disturbance is more unstable than the varicose disturbance. This implies that the varicose disturbance should not be treated as a separate route for transition, as it is completely masked by the sinuous disturbance. Therefore, only three instability mechanisms remain relevant, even-sinuous, odd-varicose and odd-sinuous. The sinuous disturbances (figure 2b,d) are clearly associated with spanwise inflection points. The varicose disturbance (figure 2c, odd TG) is associated with the wall-normal inflection at the center of the channel. This type of disturbance was investigated by us previously [5].

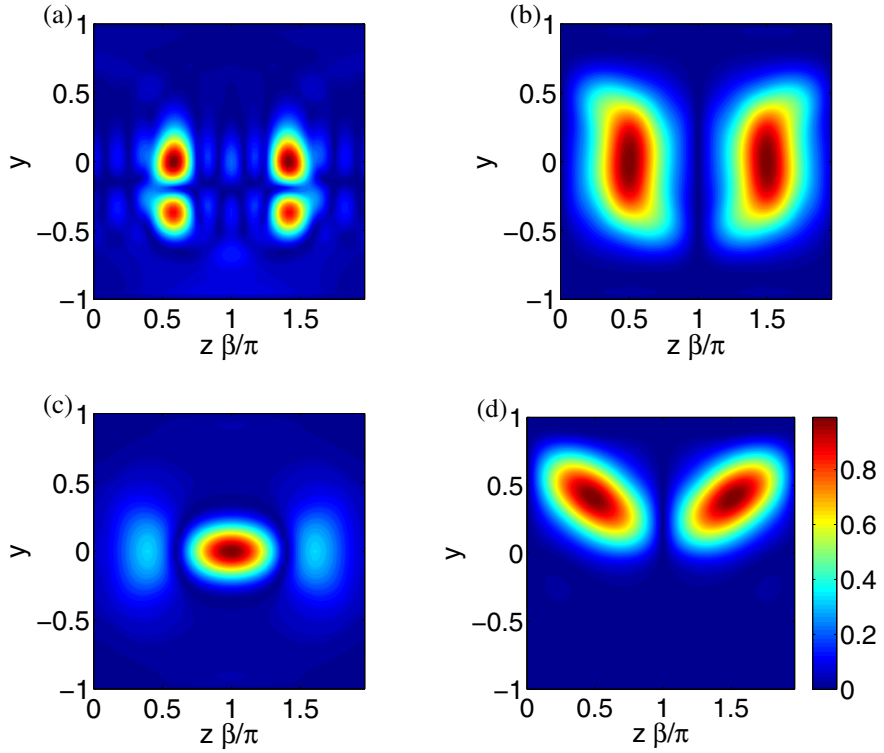

Figure 2. Magnitude of the streamwise component of the secondary disturbance corresponding to the parameters in table 2, obtained by $2d$ analysis for $Re = 1000$ and $E_0 = 10^{-4}$. (a) varicose, even TG; (b) sinuous, even TG; (c) varicose, odd TG; (d) sinuous, odd TG.

To verify the stability analysis we have simulated the evolution of above identified three disturbances in DNS. The simulation may be initiated at $t = 0$ with the analytical expressions of the four modes and the secondary disturbance. Nevertheless, as the TG is initially algebraic and the separation of time scales associated with the TG and the secondary disturbance in not valid at very short times, it is useful to initiate the simulation at some time t_0 when the TG becomes slowly varying in comparison with the growth rate of the secondary disturbance. The amplitude of the secondary disturbance has been chosen so that the fraction of energy in the secondary disturbance is 1% of the initial TG energy (e.g. for $E_0 = 10^{-4}$ the secondary disturbance adds the energy $\Delta E = 10^{-6}$ to the TG at time t_0).

The energy growth for the even-sinuous scenario is presented in figure 3a. The energy during transition is indicated by the solid red line along with the unperturbed TG scenario (without a secondary disturbance) indicated by the red dashed line. The analytical approximation of the transition scenario using the multiple scales method is given by

the solid blue line and the analytical curve for the unperturbed TG is indicated by the blue dashed line. The rapid transition occurring at $t \sim 90$ justifies the multiple time scales approach and a very good agreement is seen between the DNS and the analytical approximation. However, a significant difference in the unperturbed TG scenarios is observed. This difference results from higher order nonlinear TG interactions between the four modes which have not been accounted for in the derivation (e.g. $O(\varepsilon^3)$). Nevertheless, the good agreement between DNS and theory indicates that the additional nonlinear TG interactions do not influence the transition scenario significantly. The energy growth for the odd-varicose scenario is presented in figure 3b. The agreement in this case is very good as well. Comparing the values of the gain in this scenario with the previous one we see that the odd TG attains a gain of one order of magnitude less compared to the even TG. This further demonstrates that maximal energy gain is not essential for transition. For the odd-sinuous scenario a good agreement has been obtained as well (not shown).

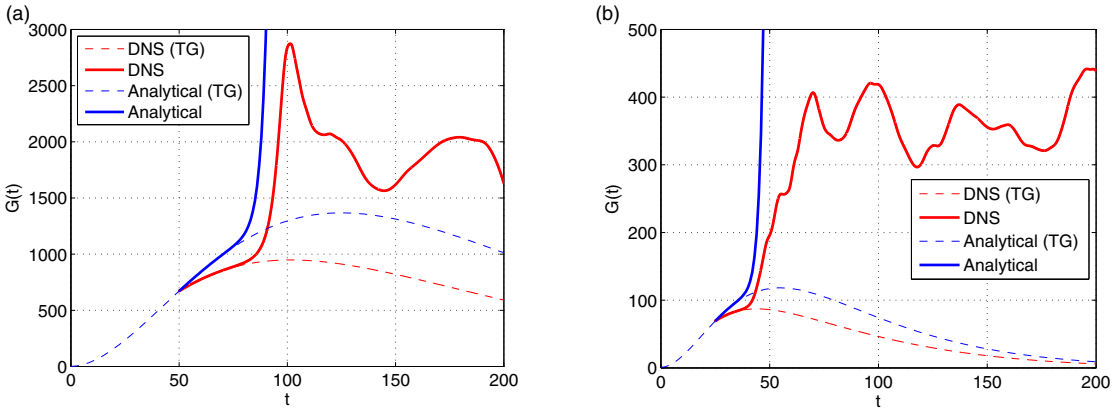

Figure 3. Energy growth during transition. Comparison between DNS (red) and analytical (blue) approximation. Unperturbed TG scenarios are indicated by the dashed lines. (a) sinuous, even TG; (b) varicose, odd TG.

As presented above, the dominant instability of the analytically modeled streaks in Couette flow is a sinuous one, associated with the spanwise inflection points. However, in several transitional experiments (e.g. channel flow [7] and pipe flow [8]) the varicose instabilities have been identified as the most dangerous ones. To understand the reason for these differences a secondary stability analysis of the experimentally generated streaks is required. For this purpose a $2d$ streaky velocity profile in Poiseuille flow is measured using a hot-wire for $Re = 1660$ and $\beta \sim 8$. The streak is generated by continuous injection through a streamwise elongated slit and the experimental setup is described thoroughly in ref. [7]. The velocity field is presented in figure 4. The 'strongest inflection' one-dimensional velocity distributions in the wall-normal (black) and spanwise (magenta) directions are superimposed on the velocity profile and the strongest inflections are encircled. A secondary stability analysis of the experimental base-flow for confirms that the varicose mode is the most unstable one for all relevant streamwise wavenumbers. The streamwise magnitude of the least stable varicose and sinuous eigenfunctions for $\alpha = 6.25$ is presented in figure 5. It can be seen that the varicose mode is associated with the wall-normal inflection whereas the sinuous mode is associated with the spanwise inflection points. The varicose mode is unstable whereas the sinuous mode is stable. Comparing the eigenfunctions to the ones presented in figure 2 for the Couette TG we see that the

eigenfunctions associated with the Couette TG span through the whole channel height while the experimental associated eigenfunctions are much more concentrated in the wall-normal direction. Thus, for the Couette even TG the wall-normal inflection point, which forms close to the wall, is unable to trigger instability at all and varicose instability is evident only for the odd TG. On the other hand, the experimentally generated streaks and their inflection points are concentrated in a certain region in the flow, which is rather far from the wall. This allows the wall-normal inflection point to trigger instability efficiently.

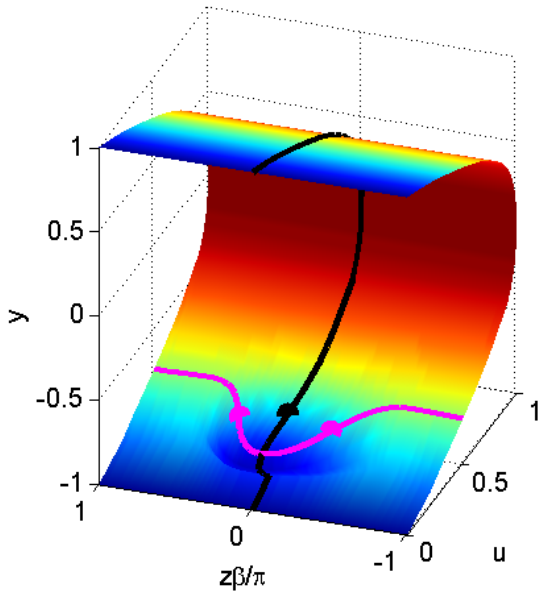

Figure 4. Experimental streaks in Poiseuille flow generated by continuous injection ($Re = 1660$ and $\beta \sim 8$). The strongest inflection $1d$ velocity distributions in the wall-normal (black) and spanwise (magenta) directions are superimposed on the velocity profile and the strongest inflections are encircled. The color indicates the magnitude of velocity.

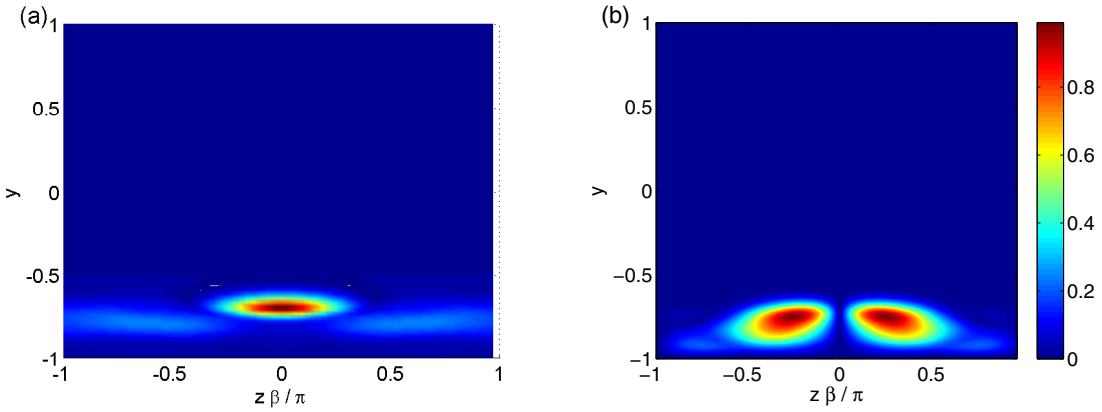

Figure 5. Magnitude of the streamwise component of the least stable varicose (a) and sinuous (b) secondary disturbances of the experimental streaks for $\alpha = 6.25$.

IV. Summary and Conclusions

The stability of streaks in has been studied analytically, numerically and experimentally. The most dangerous secondary disturbances of TG in Couette flow have been identified using the Floquet theory for the two dimensional base-flow $U(y,z)$. The parameters maximizing the growth rate are associated with the strongest inflection points, i.e. those having maximal shear, and not maximal energy gain. The optimal secondary sinuous disturbances, associated with the spanwise inflections (at the center of the channel for symmetric TG and top/bottom channel-half for antisymmetric TG), are attained for a spanwise wavenumber of $\beta \sim 3.6$ for both types of TG. The optimal varicose disturbance for the antisymmetric TG is attained for $\beta = 1.6$ and corresponds to the wall-normal inflection at the center of the channel. The routes to turbulence for the above three scenarios are explored via DNS initiated by the analytical expressions and the results are compared successfully with theoretical predictions, obtained by the multiple time scales method, verifying the latter.

Finally, the above results are compared with previous experimental results obtained in transitional pipe and Poiseuille flow experiments. The reason for the dominance of sinuous disturbances (spanwise inflections) for Couette TG is the confinement of the walls that prohibit growth of varicose disturbances for the even TG. Nevertheless, for several experimentally generated streaks the effect of the walls on the varicose disturbances (wall-normal inflection) is negligible, allowing them to become the most dominant ones.

Acknowledgments

This research was supported by the Israeli Science Foundation under Grant No. 1394/11. M. Karp would like to thank the Israeli Ministry of Science, Technology and Space for their travel support grant.

Appendix A: Amplitude correction

This appendix presents the derivation of the amplitude correction from the $O(\mu\delta)$ equations given below. The left hand side is identical to the secondary linear stability problem (ref. [5], eq. (2.6)), whereas the right hand side contains forcing terms which depend on $\boldsymbol{U}$ and $\boldsymbol{u}_d$. The $O(\mu\delta)$ equations for $\boldsymbol{u}_{dd} = (u_{dd}, v_{dd}, w_{dd})^T$ and the corresponding pressure p_{dd} are:

$$\frac{\partial u_{dd}}{\partial x} + \frac{\partial v_{dd}}{\partial y} + \frac{\partial w_{dd}}{\partial z} = 0, \tag{A 1a}$$

$$\frac{\partial u_{dd}}{\partial t} + U\frac{\partial u_{dd}}{\partial x} + v_{dd}\frac{\partial U}{\partial y} + w_{dd}\frac{\partial U}{\partial z} + \frac{\partial p_{dd}}{\partial x} - \frac{1}{Re}\boldsymbol{\nabla}^2 u_{dd} = N_a, \tag{A 1b}$$

$$\frac{\partial v_{dd}}{\partial t} + U\frac{\partial v_{dd}}{\partial x} + \frac{\partial p_{dd}}{\partial y} - \frac{1}{Re}\boldsymbol{\nabla}^2 v_{dd} = N_b, \tag{A 1c}$$

$$\frac{\partial w_{dd}}{\partial t} + U\frac{\partial w_{dd}}{\partial x} + \frac{\partial p_{dd}}{\partial z} - \frac{1}{Re}\boldsymbol{\nabla}^2 w_{dd} = N_c, \tag{A 1d}$$

where the right hand side expressions are given by:

$$N_a = -\frac{\partial u_d}{\partial \tau} - V\frac{\partial u_d}{\partial y} - W\frac{\partial u_d}{\partial z}, \tag{A 2a}$$

$$N_b = -\frac{\partial v_d}{\partial \tau} - V\frac{\partial v_d}{\partial y} - v_d\frac{\partial V}{\partial y} - W\frac{\partial v_d}{\partial z} - w_d\frac{\partial V}{\partial z}, \tag{A 2b}$$

$$N_c = -\frac{\partial w_d}{\partial \tau} - V\frac{\partial w_d}{\partial y} - v_d\frac{\partial W}{\partial y} - W\frac{\partial w_d}{\partial z} - w_d\frac{\partial W}{\partial z}. \tag{A 2c}$$

Solutions of eq. (A 1) are possible only if its right hand side is orthogonal to the conjugate of the adjoint variables which are the solutions of the homogenous adjoint equations. The corresponding solvability condition is:

$$\sum_{k=-M_z}^{M_z} \int_{-1}^{1} \left(\hat{u}^*_{a_k} N_a + \hat{v}^*_{a_k} N_b + \hat{w}^*_{a_k} N_c\right) dy = 0, \tag{A 3}$$

where $\hat{u}^*_{a_k}, \hat{v}^*_{a_k}, \hat{w}^*_{a_k}$ are the conjugate adjoint variables, the derivation of which is detailed in appendix B. Substituting the expression for the secondary disturbance (5) into the solvability condition leads to an equation for the amplitude $A(\tau)$:

$$M(\tau)\frac{dA}{d\tau} + N(\tau)A(\tau) = 0, \tag{A 4}$$

where $M(\tau)$ and $N(\tau)$ are given by:

$$M = \sum_{k=-M_z}^{M_z} \int_{-1}^{1} \left(\hat{u}^*_{a_k}\hat{u}_{d_k} + \hat{v}^*_{a_k}\hat{v}_{d_k} + \hat{w}^*_{a_k}\hat{w}_{d_k}\right) dy, \tag{A 5a}$$

$$\begin{aligned} N = \sum_{k=-M_z}^{M_z} \int_{-1}^{1} \Bigg\{ & \left(\frac{\partial \hat{u}_{d_k}}{\partial \tau} + V\frac{\partial \hat{u}_{d_k}}{\partial y} + W\frac{\partial \hat{u}_{d_k}}{\partial z}\right)\hat{u}^*_{a_k} \\ & + \left(\frac{\partial \hat{v}_{d_k}}{\partial \tau} + V\frac{\partial \hat{v}_{d_k}}{\partial y} + \hat{v}_{d_k}\frac{\partial V}{\partial y} + W\frac{\partial \hat{v}_{d_k}}{\partial z} + \hat{w}_{d_k}\frac{\partial V}{\partial z}\right)\hat{v}^*_{a_k} \\ & + \left(\frac{\partial \hat{w}_{d_k}}{\partial \tau} + V\frac{\partial \hat{w}_{d_k}}{\partial y} + \hat{v}_{d_k}\frac{\partial W}{\partial y} + W\frac{\partial \hat{w}_{d_k}}{\partial z} + \hat{w}_{d_k}\frac{\partial W}{\partial z}\right)\hat{w}^*_{a_k}\Bigg\} dy. \end{aligned} \tag{A 5b}$$

Consequently, the amplitude is given by

$$A(\tau) = A_0 \exp\left(-\int_{\tau_0}^{\tau} \frac{N(t')}{M(t')} dt'\right), \tag{A 6}$$

where A_0 is the initial amplitude at time τ_0.

Appendix B: The adjoint secondary stability problem

This appendix discusses the derivation of the adjoint secondary stability equations. As the solvability condition relies on the conjugate of the adjoint variables, it is more convenient to directly derive the conjugate adjoint equations. The equations are derived

from the regular equations in a manner similar to the one detailed in ref. [9]. First, the secondary stability equations are written in the form:

$$\frac{d\boldsymbol{A}}{dy} = \boldsymbol{H}_1\boldsymbol{A} + i\omega\boldsymbol{H}_2\boldsymbol{A}, \tag{B 1}$$

where $\boldsymbol{A} = (u, v, w, p, \Omega_x, \Omega_z)^T$ represents the regular variables and $\boldsymbol{H}_1$ and $\boldsymbol{H}_2$ are 6x6 matrices (not given here for the sake of brevity). Then, the conjugate adjoint system is given by

$$\frac{d\boldsymbol{B}^*}{dy} = -\boldsymbol{H}_1^T\boldsymbol{B}^* + i\omega\boldsymbol{H}_2^T\boldsymbol{B}^*, \tag{B 2}$$

where $\boldsymbol{B}^* = (B_1^*, B_2^*, B_3^*, B_4^*, B_5^*, B_6^*)^T$ represents the conjugate of the adjoint variables. Giving physical meaning to the components of $\boldsymbol{B}^*$, the above equations can be reduced back to a 4x4 system, the solution of which is the conjugate of the adjoint variables $u_a^*, v_a^*, w_a^*, p_a^*$:

$$\frac{\partial u_a^*}{\partial x} - \frac{\partial v_a^*}{\partial y} + \frac{\partial w_a^*}{\partial z} = 0, \tag{B 3a}$$

$$\frac{\partial u_a^*}{\partial t} + U\frac{\partial u_a^*}{\partial x} + \frac{\partial p_a^*}{\partial x} - \frac{1}{Re}\boldsymbol{\nabla}^2 u_a^* = 0, \tag{B 3b}$$

$$\frac{\partial v_a^*}{\partial t} + U\frac{\partial v_a^*}{\partial x} + \frac{\partial U}{\partial y}u_a^* - \frac{\partial p_a^*}{\partial y} - \frac{1}{Re}\boldsymbol{\nabla}^2 v_a^* = 0, \tag{B 3c}$$

$$\frac{\partial w_a^*}{\partial t} + U\frac{\partial w_a^*}{\partial x} - \frac{\partial U}{\partial z}u_a^* + \frac{\partial p_a^*}{\partial z} - \frac{1}{Re}\boldsymbol{\nabla}^2 w_a^* = 0. \tag{B 3d}$$

These equations are solved similarly to the regular secondary stability problem by a Floquet decomposition with respect to the spanwise coordinate (detailed in [5], appendix C). The calculations were verified by obtaining the same spectrum for both the regular and conjugate adjoint problems and confirmation that the eigenmodes are indeed orthogonal. In other words, if $\tilde{\boldsymbol{u}}_d$ is an eigenmode corresponding to the eigenvalue ω_1 and $\tilde{\boldsymbol{u}}_a^*$ is the conjugate of the adjoint eigenmode corresponding to ω_2, then for $\omega_1 \neq \omega_2$ the eigenmodes are orthogonal if

$$\sum_{k=-M_z}^{M_z}\int_{-1}^{1}\left(\hat{u}_{a_k}^*\hat{u}_{d_k} + \hat{v}_{a_k}^*\hat{v}_{d_k} + \hat{w}_{a_k}^*\hat{w}_{d_k}\right)dy = 0, \tag{B 4}$$

where we have defined ($\boldsymbol{q} = \boldsymbol{u}_d, \boldsymbol{u}_a^*$):

$$\tilde{\boldsymbol{q}} = \sum_{k=-M_z}^{M_z}\hat{\boldsymbol{q}}_k(t, y)e^{i\beta kz}. \tag{B 5}$$

References

[1] Blackwelder, R. F., "Analogies between transitional and turbulent boundary layers," *Phys. Fluids*, Vol. 26, 1983, pp. 2807–2815.

[2] Swearingen, J. D. and Blackwelder, R. F., "The growth and breakdown of streamwise vortices in the presence of a wall," *J. Fluid Mech.*, Vol. 182, 1987, pp. 255–290.

[3] Butler, K. M. and Farrell, B. F., "Three-dimensional optimal perturbations in viscous shear flow," *Phys. Fluids A*, Vol. 4, 1992, pp. 1637–1650.

[4] Reddy, S. C., Schmid, P. J., Baggett, J. S., and Henningson, D. S., "On the stability of streamwise streaks and transition thresholds in plane channel flows," *J. Fluid Mech.*, Vol. 365, 1998, pp. 269–303.

[5] Karp, M. and Cohen, J., "Tracking stages of transition in Couette flow analytically," *J. Fluid Mech.*, Vol. 748, 2014, pp. 896–931.

[6] Gibson, J. F., "Channelflow: A spectral Navier-Stokes simulator in C++," Tech. rep., U. New Hampshire, 2012, `Channelflow.org`.

[7] Philip, J., Svizher, A., and Cohen, J., "Scaling law for a subcritical transition in plane Poiseuille flow," *Phys. Rev. Lett.*, Vol. 98, 2007, pp. 154502.

[8] Cohen, J., Karp, M., and Mehta, V., "A minimal flow-elements model for the generation of packets of hairpin vortices in shear flows," *J. Fluid Mech.*, 2014.

[9] Tumin, A., Amitay, M., Cohen, J., and De Zhou, M., "A normal multimode decomposition method for stability experiments," *Phys. Fluids*, Vol. 8, 1996, pp. 2777–2779.